

Morphology Transitions of SDS Coatings on Single-Wall Carbon Nanotubes

Ali A. Alizadehmojarad^{†§}, Sergei M. Bachilo[†], Anatoly B. Kolomeisky[†], and R. Bruce Weisman^{*,†,‡}

[†] Department of Chemistry and the Smalley-Curl Institute, Rice University, Houston, TX 77005 United States

[‡] Department of Materials Science and NanoEngineering, Rice University, Houston, TX 77005 United States

Abstract

The morphologies of sodium dodecyl sulfate (SDS) coatings adsorbed on single-wall carbon nanotubes (SWCNTs) were investigated through molecular dynamics (MD) computations. Simulations covering a range of nanotube diameters and SDS concentrations showed regimes giving three different SDS morphologies, characterized as ordered, random, and micellar. In the ordered structures, which were formed at the lowest SDS concentrations, nanotubes were coated with a partial monolayer of SDS molecules whose alkyl tails were aligned parallel to the nanotube axis. Higher SDS concentrations gave the random coating morphology, with a partial monolayer of more closely packed and poorly aligned adsorbed molecules. At the highest concentrations, spheroidal micellar clusters of SDS formed on the nanotube surface. The morphologies were quantitatively characterized by computed distribution functions of SDS alkyl chain orientation and radius of gyration. A machine learning method was also applied to determine aggregation numbers of SDS micelles in these colloidal systems.

Keywords: SDS adsorption; nanotube surfactants, molecular dynamics simulation, machine learning for colloid science

Introduction

Single-wall carbon nanotubes (SWCNTs) are a family of one-dimensional nanomaterials whose members display a wide range of electronic properties ranging from metallic to semiconducting. The π -electronic structure of a particular nanotube is determined by its diameter and roll-up angle, which can be found from the pair of integers, (n,m) , that label its structural species.¹ Aqueous suspensions of individualized SWCNTs are widely used in basic research and applications. Because SWCNTs are highly hydrophobic, these suspensions are prepared with the aid of noncovalent surfactant or polymeric coatings,²⁻⁵ which often play important roles in the behavior of suspended nanotubes in sorting processes and biological environments.⁶⁻⁸ It is therefore important to understand the nature of adsorbed coatings on individual SWCNTs.

One of the most widely used SWCNT coatings is the common surfactant sodium dodecyl sulfate (SDS). Resolving and understanding the detailed morphology and affinities of SDS coatings is particularly challenging for experimental and theoretical research⁹⁻¹⁶ because of the surfactant molecules' small size, flexible structure, and weak van der Waals interactions with the nanotube surface.^{17,18} Surfactant concentration, solution ionic strength, pH, temperature, and nanotube diameter are variables that can affect the structures of SDS coatings on SWCNT surfaces.^{13,16,19,20} In the absence of reliable experimental data on the numbers of SDS molecules adsorbed on suspended SWCNTs, insights may be obtained from simulations using molecular dynamics (MD), which is a robust tool for investigating molecular scale phenomena such as the morphology of surfactant micelles.²¹ Prior MD studies applied to SDS coatings on SWCNTs have reported surfactant molecules forming both random and micellar morphologies, consistent with some experimental results.^{10,13,14} However, to our knowledge, previous research has not investigated the factors controlling morphologies of SDS molecules on nanotube surfaces. In the present study we computationally explore how surfactant concentration and nanotube diameter determine the structures of adsorbed SDS coatings on SWCNTs and use our findings to estimate an effective morphology phase diagram.

Computational Methods

We performed MD simulations using NAMD 2.13 software.²³ All interaction parameters were obtained from CHARMM force fields, while the TIP3P model was used for water species.^{24,25} Construction of simulation systems and the visualization and analysis of results were managed by

VMD software.²⁶ To solvate systems in water and neutralize them with sodium counter ions, we applied the VMD plugins Solvate and Ionize, respectively. All simulation systems had identical dimensions ($13.6 \times 13.6 \times 18 \text{ nm}^3$) and correspondingly almost the same number of water molecules (~96,396). The only differences among them were the number of SDS molecules and the SWCNT species. Our recently published paper introduced a new method to quantify DNA/SWCNT mass ratios.²⁷ However, the corresponding SDS/SWCNT mass ratios are more challenging to measure, and no experimental values are available. Lacking experimental guidance on the SDS surface coverage on SWCNTs, we simulated systems containing 50, 100, 200, 300, 400, 600, or 800 SDS molecules to represent a wide range of SDS concentrations and SDS/SWCNT mass ratios. The SWCNT chiralities of interest here were (5,4), (6,5), (8,7) and (10,9), with respective diameters (based on atomic centers) of 0.62, 0.757, 1.032, and 1.307 nm. Calculations of their total surface areas took into account the carbon atom van der Waals radius of ~1.7 Å. We used nanotube segments ~16 nm long for all chiralities, containing 1182, 1456, 1956, and 2492 carbon atoms for (5,4), (6,5), (8,7) and (10,9), respectively. Figure S1 displays the initial configuration of a 16 nm segment of (10,9) covered by 800 SDS molecules before equilibration and before solvation by water. The other systems, with smaller numbers of SDS molecules and different SWCNT chiralities, were constructed by modifying this system and then solvating with water. All MD simulation systems were run in the NPT ensemble at 1 bar pressure and a temperature of 300 K. Long-range Coulomb interactions were evaluated using the Particle Mesh Ewald (PME)²⁸ method under periodic boundary conditions in all directions. The integration time step was 2.0 fs for all simulations, and 5000 steps of energy minimization were performed before production runs of at least 100 ns.

To compute the aggregation numbers of free and adsorbed SDS micelles, we developed a method based on unsupervised machine learning. This method applies a three-dimensional K-means clustering algorithm, which is a suitable approach for recognizing and characterizing nearly spherical clusters such as SDS micelles formed around a centroid. In our custom Python code, the number of clusters or aggregates in simulations with SDS and SDS-coated SWCNTs is either given or is computed by optimization, and the aggregation numbers of free and adsorbed SDS micelles are then calculated. Our dataset was constructed by computing the x, y and z center of mass (COM) coordinates of all SDS molecules in each MD simulation and then building a COM trajectory for the last 500 frames. The data in our dataset were not labelled and the aggregation numbers for all

identified clusters were calculated for each frame. The standard deviation of aggregation number for each cluster was first evaluated from the last 500 frames and then this value was used to represent the standard deviation of all free or adsorbed clusters. Figure S1b shows adsorbed SDS clusters, Figure S1c shows free SDS clusters, and the attached video (see Supporting Information) shows free and adsorbed clusters for the last 500 frames.

Results and Discussion

We presume that SDS-nanotube interactions can be properly modeled as van der Waals forces, since SDS lacks aromatic rings and cannot have π – π stacking interactions with SWCNTs. Despite this simplification, SDS morphology on SWCNT surfaces is complex because of possible dependencies on nanotube diameter, SDS concentration, solution ionic strength, pH, and temperature. To keep the scale of our study manageable, we varied only nanotube diameter and SDS concentration in these simulations. The simulated SDS concentration ranged from 0.7 to 12 % w/v, as compared to the experimental critical micelle concentration (CMC) of 0.237 % in water.^{28,29} By increasing the number of SDS molecules in the simulations, we were able to model the impact of SDS/SWCNT mass ratio on SDS morphology. We observed that the critical SDS concentration needed to form free micelles (the CMC) increases when nanotubes are present. Also, at SDS/SWCNT mass ratios lower than ~2, SDS does not form micellar structures on SWCNT surfaces even at concentrations above the normal CMC. Instead, the SDS adsorbs to form other morphologies, termed ordered or random, on the nanotube surface. We also explored the effect of nanotube curvature and diameter on the adsorbed SDS morphologies by performing simulations on (5,4), (6,5), (8,7) and (10,9) SWCNTs, which have diameters ranging from 0.62 to 1.307 nm.

Effect of SDS concentration. We find that the SDS/SWCNT mass ratio is the dominant factor determining SDS coating structures on nanotube surfaces. The MD snapshots in Figure 1 show how SDS morphology is correlated with the SDS/SWCNT mass ratio, which was varied in our simulations by changing the number of SDS molecules present with a single SWCNT segment. We identified three different morphology types upon increasing the number of SDS molecules from 50 to 400 with a ~16 nm segment of (5,4) SWCNT. Type 1 (Ordered Monolayer): At the lowest surfactant concentration (0.76% w/v), SDS molecules form a moderately ordered monolayer on the nanotube surface, with alkyl chains nearly aligned parallel to the nanotube axis except at some interaction sites between neighbors attributed to the low available surface area and

high curvature of the (5,4) SWCNT. In this morphology, the SWCNT surface is not fully covered and a portion is exposed to water. Type 2 (Random Monolayer): On doubling the SDS number to 100, a denser morphology forms that is still a monolayer but shows SDS molecules adsorbed with orientational disorder of the alkyl chains. This random structure more fully covers the SWCNT surface, and the charged tails of SDS molecules stand out of the monolayer coating, as was suggested in previous reports.^{9,12–14} Type 3 (Micellar Clusters): In the presence of still more SDS molecules in the simulations, we found the onset of a morphology that shows distinct adsorbed micelle-like clusters adsorbed on the SWCNT surface. For (5,4) SWCNTs, these appeared at an SDS number of 150. In simulations with the number of SDS molecules increased to between 150 and 300, the number of adsorbed clusters remained the same but their sizes grew according to the SDS concentration. Further increases in available SDS resulted in the formation of free micelles (not adsorbed onto the nanotube) with little change to the adsorbed micellar clusters.

These observations suggest that the CMC of SDS in the presence of nanotubes is much higher than in pure water (~0.82 mM). Note that all of our results were obtained at simulated SDS concentrations greater than that CMC value. The increase in apparent CMC may be traced to the SWCNT hydrophobicity, which provides a surface for low energy adsorption by the SDS alkyl chains. This adsorption then lowers the effective concentration of dissolved SDS molecules available to form micelles. Figure 1 shows that four SDS micelles formed on the surface of the (5,4) nanotube segment when we included 400 SDS molecules (~6 % w/v) in the simulation box. This finding is consistent with the experimental correlation between micelle aggregation number and SDS concentration in water without nanotubes.^{28,29} However, that reported correlation is not strong, with micelle aggregation numbers near 90 for ~4.5 % w/v (300 SDS in the present study) and also for ~6 % w/v (400 SDS).^{28,29} To further investigate this effect, we increased the number of SDS molecules in our simulations to 600 (9 % w/v) and 800 (12 % w/v). This again led to four SDS micelles on the (5,4) segment (see Figure 1). However, at these higher concentrations, the simulation showed the presence of free micelles in solution in addition to adsorbed micelles having the same aggregation number as at lower concentrations.

Effect of SWCNT diameter. We supplemented our (5,4) computations with similar MD simulations of SDS adsorption on three larger diameter SWCNTs: (6,5), (8,7) and (10,9). The snapshots in Figure 1 illustrate the morphologies found for SDS on (5,4) and (10,9) SWCNTs, the smallest and largest diameter species studied here. The Type 1 (ordered) morphology was observed

on (5,4) SWCNTs at SDS/SWCNT mass ratios below 0.93 (<50 SDS molecules), as compared to 0.88 (<100 SDS) for (10,9) nanotubes. We found the Type 2 (random) morphology on (5,4) nanotubes at an SDS/SWCNT mass ratio of 1.87 (100 SDS), compared to 1.77 (200 SDS) on (10,9). The onset of Type 3 (micellar cluster) adsorption on (5,4) and (10,9) SWCNTs appeared at SDS/SWCNT mass ratios of 2.8 (150 SDS) and 2.21 (250 SDS), respectively. At higher SDS concentrations, we found fewer free (dissolved) micelles and more adsorbed SDS molecules on the (10,9) segment as compared to (5,4) (see Figure 1). These observations show that, although the SDS concentrations in these two systems were both above the CMC, SDS micellar structures were formed on (10,9) at a lower SDS/SWCNT ratio than for (5,4) SWCNTs.

As expected, our simulations find that the extent of SDS adsorption on SWCNTs increases with total SDS concentration. Figure 2a shows that the number of adsorbed SDS molecules per

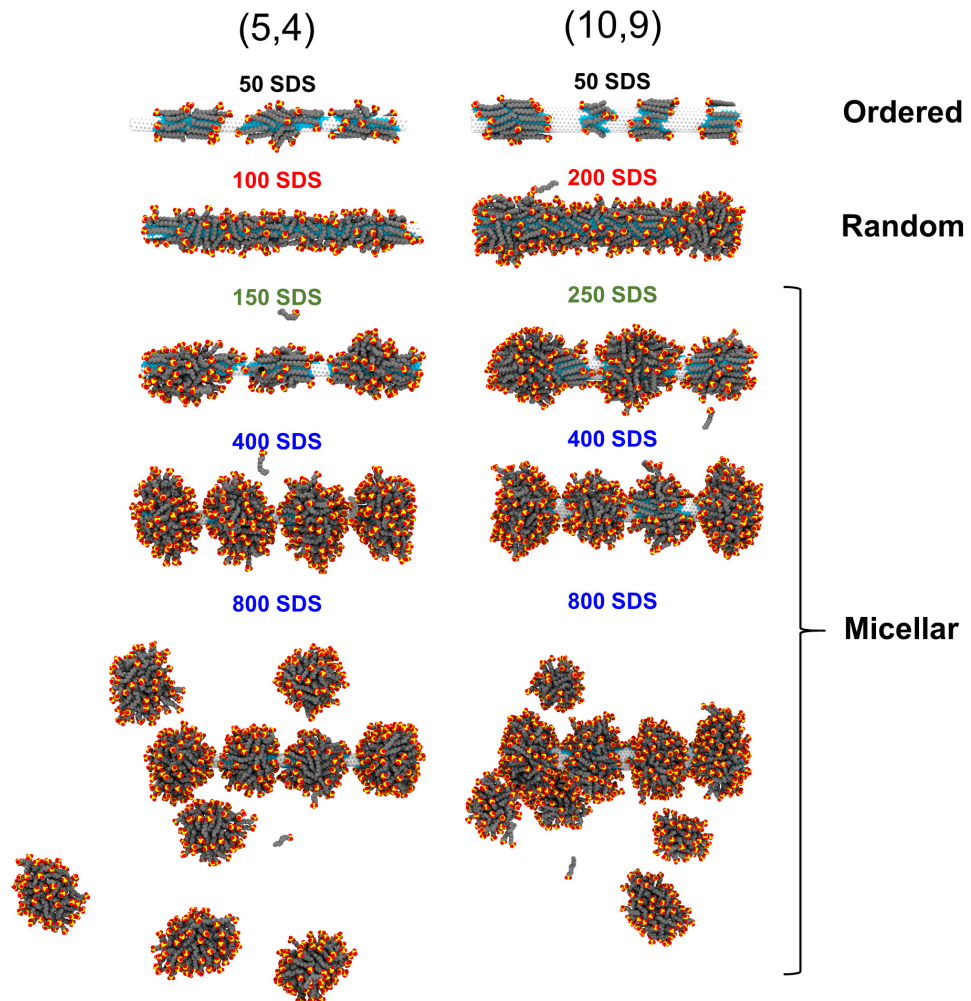


Figure 1. Typical snapshots from equilibrated molecular dynamics (MD) simulations of aqueous SDS with segments of (5,4) and (10,9) SWCNTs. Nanotube carbon atoms are colored white; SDS carbon atoms are grey; oxygen atoms are red; and sulfur atoms are yellow. The label above each image gives the number of SDS molecules present in the simulation. The corresponding SDS/SWCNT mass ratios for (5,4) are, from top to bottom: 0.93, 1.87, 2.80, 7.48, and 15.0. For the (10,9) systems, those mass ratios are 0.44, 1.77, 2.21, 3.55, and 7.10.

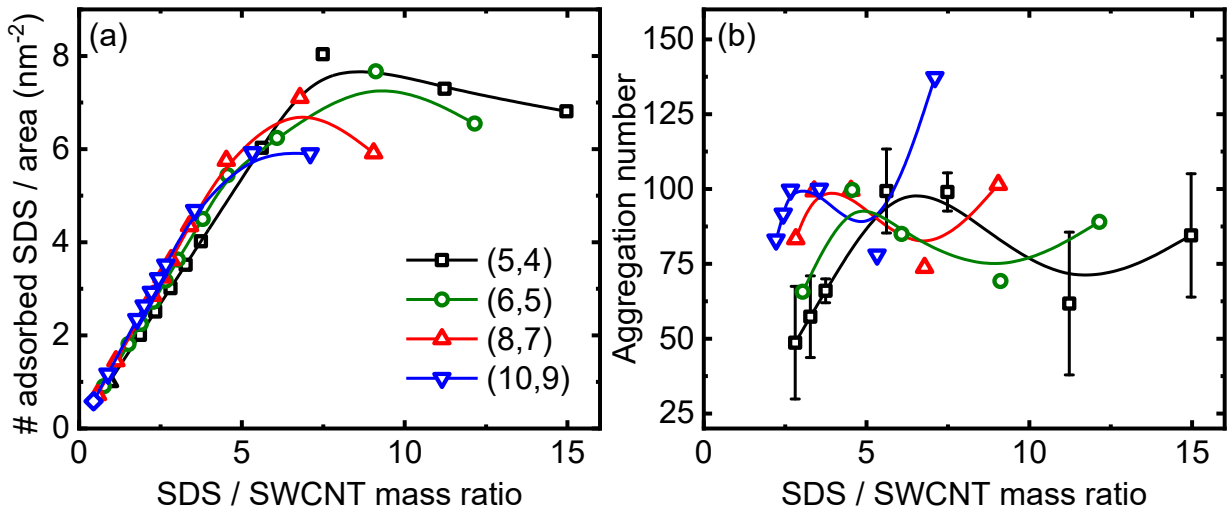


Figure 2. (a) Numbers of adsorbed SDS molecules per unit surface area of (5,4), (6,5), (8,7) or (10,9) SWCNTs plotted vs SDS/SCNT mass ratios. (b) Aggregation number of SDS micellar structures on (5,4), (6,5), (8,7) and (10,9) SWCNTs plotted vs SDS/SCNT mass ratio. The error bars (shown only for (5,4)) are based on standard deviations of aggregation numbers of three or four micelles on these species. In both frames, black, red, green, and blue curves denote (5,4), (6,5), (8,7) and (10,9) chiralities, respectively.

unit SWCNT surface area increases linearly and almost independently of nanotube diameter at low concentrations but with diameter-dependent deviations at high SDS concentrations where free micelles begin to appear. The range of linear behavior varies inversely with nanotube diameter. Figure S2 presents the same data as Figure 2a except that it correlates the number of adsorbed SDS molecules with the total number of SDS molecules in the simulation, without normalizing either to SWCNT mass or surface area. This figure suggests that the total amount of adsorbed SDS on large diameter SWCNTs is greater than on small diameter SWCNTs when free micelles are present beyond the linear region. Figure S2b is another representation of the same data, showing that large diameter SWCNTs accommodate greater numbers of SDS molecules and correspondingly have a higher saturation limit for adsorbed SDS than small diameter SWCNTs, even at the same SDS/SCNT mass ratio. We note that although the geometrical diameter of a SWCNT is proportional to its mass per unit length, its adsorption diameter (defining the surface area) is larger because of the carbon van der Waals radius, so surface area is not proportional to mass. The number of adsorbed SDS molecules per nanotube surface area is greater for small diameter

SWCNTs than large diameter ones in the saturation regime (see Figure 2a). Below saturation, both the number of adsorbed SDS per unit area and the absolute number of adsorbed SDS molecules are greater for large diameter SWCNTs than for small diameter ones at the same total SDS/SWCNT mass ratio.

We also find that SWCNT diameter affects the aggregation number of the Type 3 adsorbed SDS micellar structures. Figure 2b shows two main regimes corresponding to the absence and presence of free dissolved SDS micelles. In the first (low concentration) regime, the aggregation number of the adsorbed micellar structures increases with nanotube diameter and with the SDS/SWCNT mass ratio. As that ratio increases, the aggregation number of the adsorbed micellar structures first drops and then increases when free SDS micelles form, with greater values for the larger diameter SWCNTs. Although these aggregation number results have relatively large statistical uncertainties, they are consistent with our findings from MD simulations of smaller SWCNT/SDS systems. The observed pattern seems consistent with the above discussion about larger SWCNT diameters accommodating more SDS molecules. Previous studies of SDS in the absence of nanotubes found that micelle aggregation numbers are directly correlated with SDS concentration, varying between 53 and 110 for concentrations from 30 to 110 mM at room temperature.^{28,29} Figures S3a-b display the aggregation numbers found from our MD simulations versus total number of SDS molecules and SDS concentration (mM). The aggregation numbers are in relatively good agreement with the experimental values for pure SDS solutions, except for the local minimum at the transition from one morphology regime to another, where the aggregation number is ~70 on the SWCNT surface versus ~100 in the SDS bulk solution^{28,29} at 80 mM SDS concentration. We attribute this difference to nucleation on the SWCNT surfaces.

Characterization of SDS coating morphologies on SWCNTs. In Figure 3a we display typical MD snapshots of a (10,9) SWCNT segment coated with the three SDS morphologies identified in this study. These ordered, random, and micellar SDS patterns were observed for simulations with 50, 200, and >250 SDS molecules, respectively. Figure 4 shows a surface plot illustrating the regimes for these three SDS morphologies as a function of nanotube diameter and total SDS/SWCNT mass ratio. The z-axis in this plot is the SDS / SWCNT mass ratio including only adsorbed SDS molecules. To quantitatively characterize the morphologies, we computed two distribution functions representing features of the adsorbed SDS molecules:

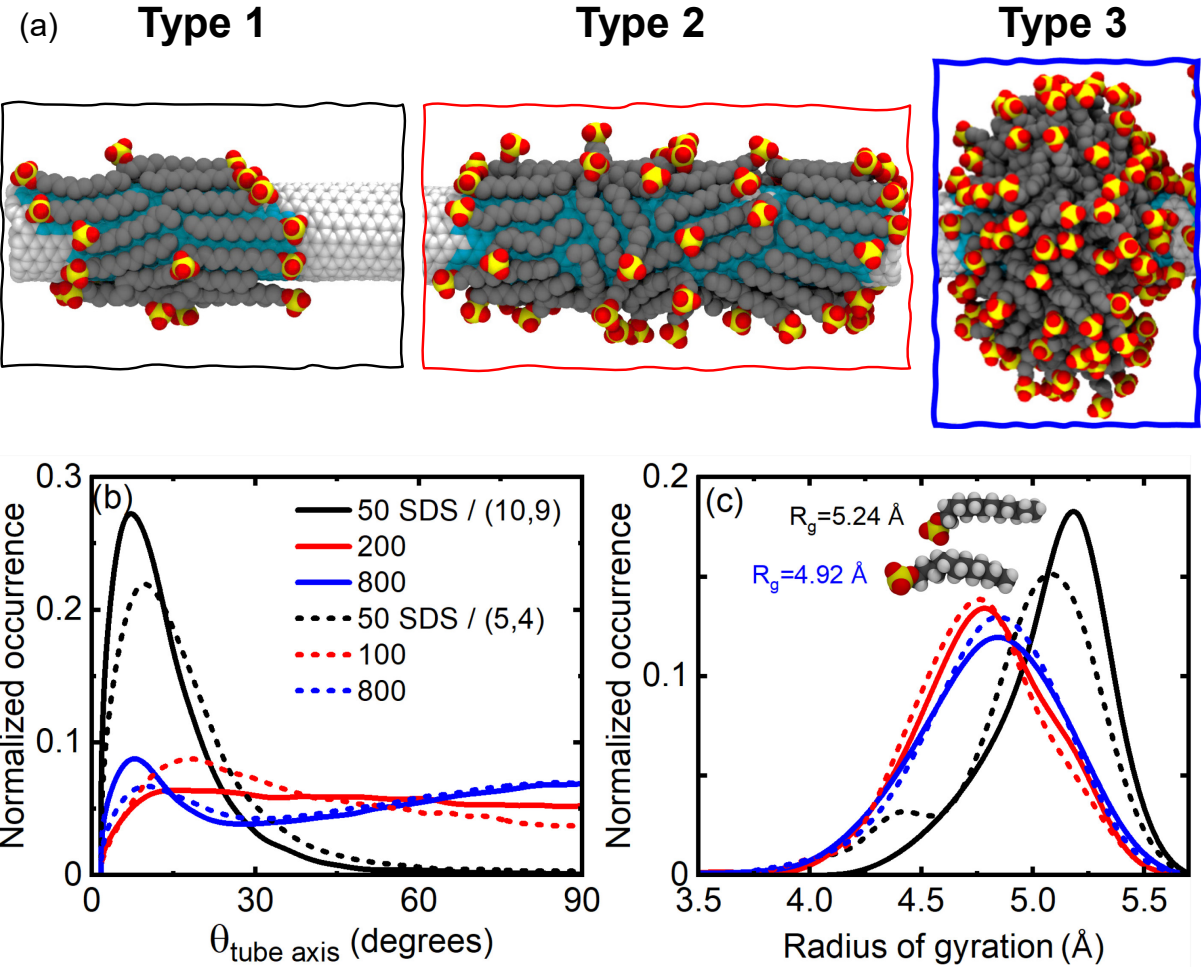


Figure 3. (a) Representative zoomed-in MD snapshots of ordered, random, and micellar morphologies of SDS adsorbed on a (10,9) SWCNT. Nanotube carbon atoms and SDS carbon, oxygen and sulfur atoms are shown in white, gray, red and yellow colors, respectively. (b) Distribution plots for the angle between each SDS alkyl chain and the nanotube axis ($\theta_{\text{tube axis}}$) for (10,9) (solid lines) and (5,4) (dashed lines) SWCNTs with 50, 100, 200, or 800 SDS molecules, as shown in the legend. (c) Distribution plots for the radius of gyration (R_g) of SDS molecules in the systems of panel (b), with the same legend. Insets show typical bent and linear SDS structures, with corresponding R_g values.

1) $\theta_{\text{tube axis}}$, the angle between a hydrocarbon tail and the SWCNT axis; and 2) R_g , the SDS molecule's radius of gyration. The latter decreases as the hydrocarbon chain is deformed away from a linear structure. Figures 3b and 3c plot those two distribution functions for our smallest and largest SWCNT diameters. Figure 3b shows that simulations with 50 SDS molecules on a 16 nm segment of either (5,4) or (10,9) led to strong alignment of adsorbed SDS chains parallel to the

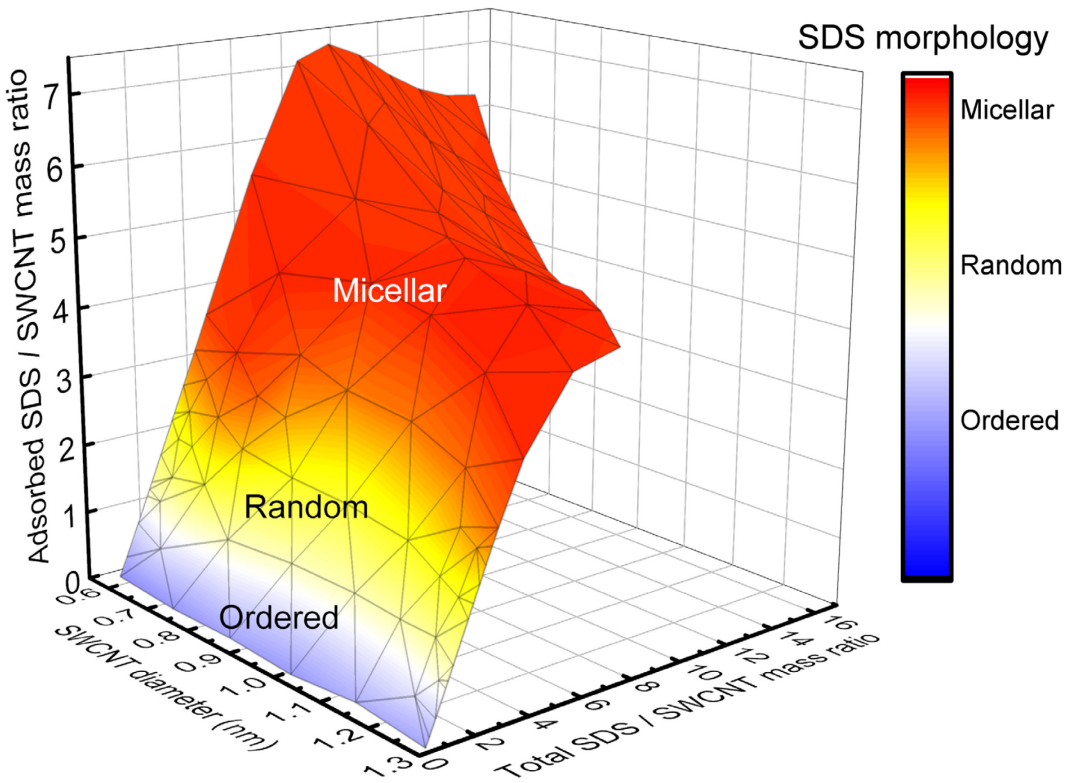


Figure 4. Surface plot showing the morphology phase diagram computed by combining all of the molecular dynamics simulations. The three color-coded structural regimes are shown as a function of dimensionless total SDS / SWCNT mass ratio and of SWCNT diameter. The z-axis represents the SDS / SWCNT mass ratio including only adsorbed SDS molecules.

tube axis (probability maximum at $\theta_{\text{tube axis}} = \sim 70^\circ$). This alignment is a signature of the ordered (Type 1) morphology. In the case of (5,4), the SDS alignment is less complete, giving a $\theta_{\text{tube axis}}$ distribution with a lower peak amplitude and a maximum angle further from zero. A snapshot of this morphology is shown in Figure 1. As was proposed in previous reports,^{12–14} these ordered structures with SDS molecules aligned along the nanotube axis involve SDS alkyl chains extended on the surface. This nearly full extension gives them large values of R_g (near 5.24 Å), as seen in the distribution plotted in Figure 3c and illustrated in the inset of that figure. Figures S4 and S5 suggest that an ordered morphology was also formed with 50 SDS around (6,5) and (8,7). For simulations with 50 SDS molecules and a (5,4) SWCNT, we found a slightly smaller peak R_g value that indicates a less ordered adsorbate structure.

At the higher concentrations of SDS that give the morphology we classify as random (Type 2), the R_g distribution broadens from the presence of two overlapping components that indicate a blend

of extended and slightly bent SDS alkyl chains. A structure for a slightly bent SDS molecule with an R_g value of ~ 4.9 Å is illustrated as an inset in Figure 3c. The Type 2 morphology also gives much less average alignment of SDS alkyl chains with the nanotube axis, as can be seen in the flattened $\theta_{\text{tube axis}}$ distributions in Figure 3b for 200 SDS molecule on (10,9) or 100 SDS on (5,4). Distributions for intermediate SWCNT diameters are plotted in Figures S4 and S5.

The Type 1 and lower coverage Type 2 morphologies have gaps between SDS-coated regions that leave portions of the nanotube surface exposed to solvent (see Figure 1). However, in higher coverage Type 2 structures, as for the simulation with 200 SDS molecules on (10,9), no gaps are apparent. Higher adsorbed SDS densities also lead to bending of the alkyl tails, as shown by lower values for maxima in the R_g distributions.

Simulations with still higher SDS concentrations show a third morphology, adsorbed micellar clusters (Type 3). A representative snapshot of this structure on a (10,9) nanotube is displayed in Figure 3a. The $\theta_{\text{tube axis}}$ distribution curve for 800 SDS molecules in Figure 3b indicates that the micellar morphology on (5,4) or (10,9) likely comprises a blend of two phases, since it shows two broad peaks at $\sim 7^\circ$ and $\sim 90^\circ$. The $\sim 7^\circ$ peak represents an aligned set of SDS molecules adsorbed at the SWCNT surface, whereas the second peak comes from SDS chains located in the bulk of the micellar cluster. Blends of these two phases were observed for all four of the studied nanotube structures, (5,4), (6,5), (8,7), and (10,9) (see also Figure S4). The presence of two structural subsets in the adsorbed micelles is also consistent with the broad R_g distribution curves, which have maxima between the values found for the ordered and random SDS morphologies (see Figures 3c and S5).

We further investigated the SDS micellar structure as a function of radial distance from the nanotube surface. Figure 5a illustrates an MD simulation snapshot for a ~ 16 nm segment of (10,9) SWCNT with 800 SDS molecules, which form both adsorbed and free micelles. For clarity, this figure includes only one of the five free SDS micelles shown in Figure 1. Below the free micelle image we show the SWCNT surface with its four adsorbed micellar clusters drawn as partly transparent to reveal their innermost layer of SDS molecules at the SWCNT surface. It can be seen that this inner layer resembles the ordered morphology, with SDS alkyl chains elongated and commonly aligned along the tube axis. Figures 5b,c plot the values for $\theta_{\text{tube axis}}$ and R_g of all of the adsorbed SDS alkyl chains as a function of their radial distance from the surface of (5,4) or (10,9) SWCNTs. Comparable graphs for (6,5) and (8,7) SWCNTs are shown in Figures S6a and S6b. For

all studied chiralities, values of $\theta_{\text{tube axis}}$ increase markedly from $\sim 7^\circ$ (ordered morphology) at the nanotube surface to $>60^\circ$ (randomly oriented) at the boundary between the SDS micellar cluster and water. Correspondingly, R_g values for the SDS alkyl chains decrease from approximately 5.3 Å (elongated) at the nanotube surface to 4.8 Å (bent) at the outer boundary of the clusters (Figure 5c).

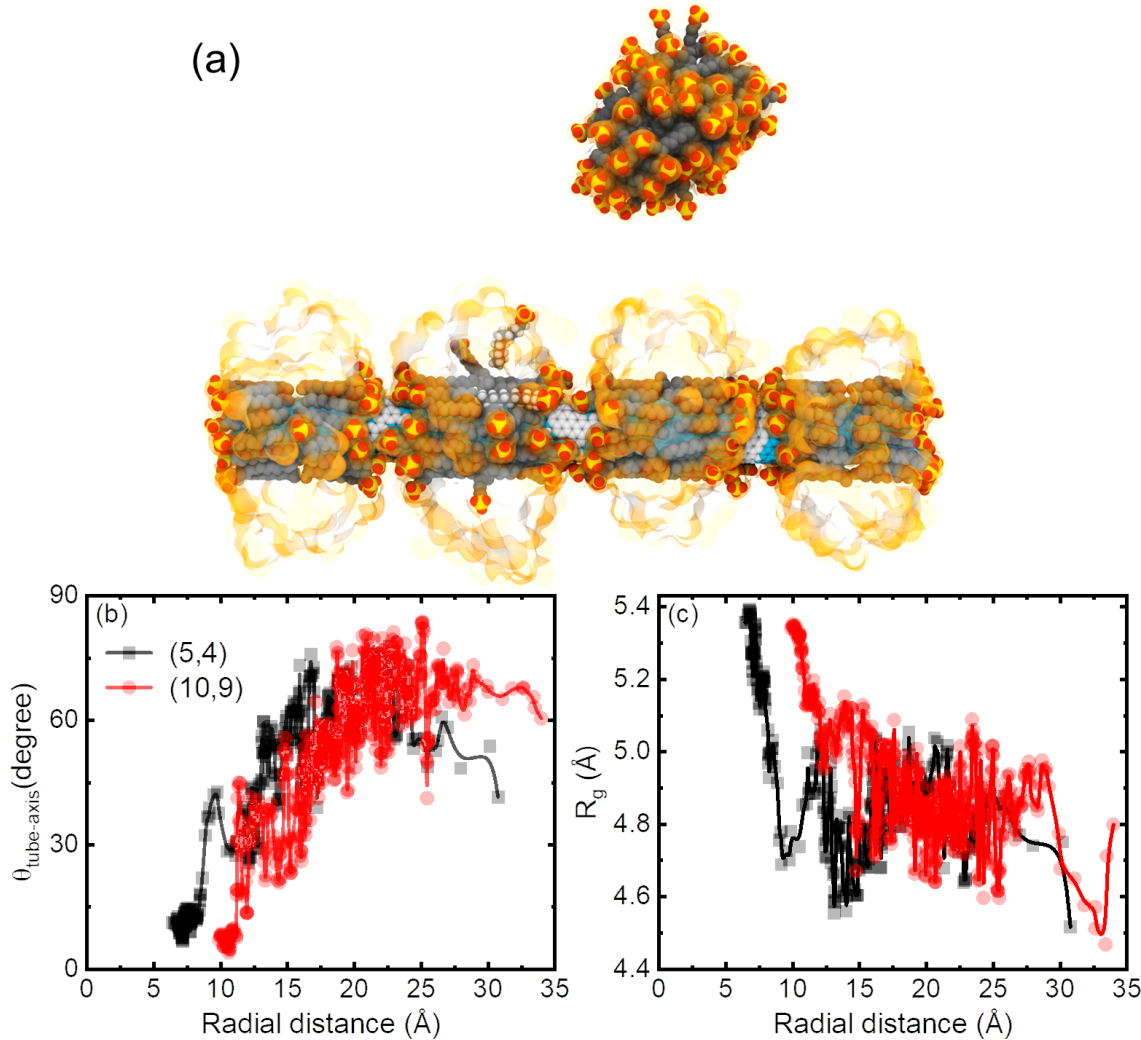


Figure 5. (a) A snapshot from a molecular dynamics simulation with 800 SDS molecules and a (10,9) SWCNT segment after equilibration. Only one of five free SDS micelles is shown. The four transparent point-cloud regions drawn in orange represent four SDS micellar clusters adsorbed on the nanotube. The innermost layer in those clusters is displayed in vdW representation to illustrate the presence of an ordered SDS morphology at the nanotube surface. Randomly oriented SDS molecules are present in the bulk of the clusters. The color scheme used here is the same as in Figure 3. (b) Angles between all SDS alkyl tails and the SWCNT axis ($\theta_{\text{tube axis}}$) plotted vs radial distance from the SWCNT surface for (5,4) (black) and (10,9) (red) SWCNTs. (c) Radii of gyration (R_g) for all SDS molecules plotted vs radial distance from the SWCNT surface for (5,4) (black) and (10,9) (red) SWCNTs. Radial distance is defined as the distance between the center of mass of each SDS molecule and the nanotube surface.

This difference reflects deformations caused by interactions among SDS chains in the interior of the micellar clusters. We also note the presence of gaps along the SWCNT surface between adjacent SDS clusters. The snapshots in Figure S7, which include Na^+ counter ions, show a number of these ions occupying positions near the SWCNT surface in those gaps. It seems possible that simulations in which SDS is not assumed to be fully ionized may show a modified clustering morphology at high concentrations.

Conclusions

We have used molecular dynamics simulations to investigate the morphologies of adsorbed SDS coatings on a range of SWCNT diameters over a range of SDS concentrations. From our results we identified three distinct morphologies: ordered, random, and micellar. In the ordered morphology, an incomplete monolayer of SDS alkyl chains are largely aligned parallel to the nanotube axis; the random morphology shows a higher density monolayer with poor alignment of SDS molecules along the axis; and the micellar morphology shows SDS clusters adsorbed to the SWCNT surface. The observed morphology is determined by the combination of SDS concentration and nanotube diameter, as larger diameter SWCNTs require more SDS molecules in the simulations to acquire a denser coating structure. In the regime where adsorbed micellar clusters are observed, the number of clusters and their aggregation numbers are modulated by the SDS concentration and by SWCNT diameter. Higher SDS concentrations give a larger number of micelles than lower SDS concentrations, and larger diameter SWCNTs tend to show clusters with higher aggregation numbers. We characterized adsorbed SDS morphologies by computing the distribution functions of their alkyl chain orientations and radii of gyration. Analysis of these parameters as a function of distance from the nanotube surface revealed that micellar clusters consist of an ordered layer at the nanotube surface underneath randomly oriented SDS molecules comprising the bulk of the cluster.

ASSOCIATED CONTENT

Supporting Information. Illustrations of initial MD structures; cluster analyses for adsorbed and free SDS micelles; plots of adsorbed SDS vs total SDS and SDS/SWCNT mass ratio; plots of SDS aggregation number vs total SDS and SDS concentration; distributions of angles and radii of gyration for SDS adsorbed at various SDS/SWCNT ratios on all studied (n,m) species; plots of angles and radii of gyration vs radial distance for SDS molecules in micellar clusters on (6,5) and

(8,7) SWCNTs; MD snapshots that include water and sodium ions for a (10,9) SWCNT with adsorbed micellar clusters; a video showing images from 500 MD frames with automatically identified free and adsorbed micellar structures.

AUTHOR INFORMATION

Corresponding Author

* E-mail: weisman@rice.edu

Present Address

§ A.A.A.: Massachusetts Institute of Technology, Cambridge, MA 02139, United States

ORCID

Ali A. Alizadehmojarad: 0000-0001-6806-5415

Sergei M. Bachilo: 0000-0001-5236-1383

Anatoly B. Kolomeisky: 0000-0001-5677-6690

R. Bruce Weisman: 0000-0001-8546-9980

NOTES

The authors declare no competing financial interests.

ACKNOWLEDGMENTS

This research was supported by a grant to R.B.W. from the National Science Foundation (CHE-2203309) and grants to A.B.K. from the Welch Foundation (C-1559) and from the Center for Theoretical Biological Physics sponsored by the National Science Foundation (PHY-2019745). We are also grateful to Pittsburgh Supercomputing Center (PSC) and San Diego Supercomputer Center (SDSC) for providing computational resources.

REFERENCES

- (1) Reich, S.; Thomsen, C.; Maultzsch, J. *Carbon Nanotubes: Basic Concepts and Physical Properties*; John Wiley & Sons: Hoboken, 2008.
- (2) Wenseleers, W.; Vlasov, I. I.; Goovaerts, E.; Obraztsova, E. D.; Lobach, A. S.; Bouwen, A. Efficient Isolation and Solubilization of Pristine Single-Walled Nanotubes in Bile Salt Micelles. *Adv. Funct. Mater.* **2004**, *14* (11), 1105–1112.
- (3) Islam, M. F.; Rojas, E.; Bergey, D. M.; Johnson, A. T.; Yodh, A. G. High Weight Fraction Surfactant Solubilization of Single-Wall Carbon Nanotubes in Water. *Nano Lett.* **2003**, *3*, 269–273.
- (4) Moore, V. C.; Strano, M. S.; Haroz, E. H.; Hauge, R. H.; Smalley, R. E.; Schmidt, J.; Talmon, Y. Individually Suspended Single-Walled Carbon Nanotubes in Various Surfactants. *Nano Lett.* **2003**, *3* (10), 1379–1382.
- (5) Nish, A.; Hwang, J. Y.; Doig, J.; Nicholas, R. J. Highly Selective Dispersion of Single-Walled Carbon Nanotubes Using Aromatic Polymers. *Nat. Nanotechnol.* **2007**, *2* (10), 640–646.
- (6) O’Connell, M. J.; Bachilo, S. M.; Huffman, C. B.; Moore, V. C.; Strano, M. S.; Haroz, E. H.; Rialon, K. L.; Boul, P. J.; Noon, W. H.; Kittrell, C.; et al. Band Gap Fluorescence from Individual Single-Walled Carbon Nanotubes. *Science* **2002**, *297*, 593–596.
- (7) Bachilo, S. M.; Strano, M. S.; Kittrell, C.; Hauge, R. H.; Smalley, R. E.; Weisman, R. B. Structure-Assigned Optical Spectra of Single-Walled Carbon Nanotubes. *Science* **2002**, *298* (5602), 2361–2366.
- (8) Zheng, M.; Jagota, A.; Semke, E. D.; Diner, B. A.; McLean, R. S.; Lustig, S. R.; Richardson, R. E.; Tassi, N. G. DNA-Assisted Dispersion and Separation of Carbon Nanotubes. *Nat Mater* **2003**, *2* (5), 338–342.
- (9) Xu, Z.; Yang, X.; Yang, Z. A Molecular Simulation Probing of Structure and Interaction for Supramolecular Sodium Dodecyl Sulfate/Single-Wall Carbon Nanotube Assemblies. *Nano Lett.* **2010**, *10* (3), 985–991.
- (10) Yurekli, K.; Mitchell, C. A.; Krishnamoorti, R. Small-Angle Neutron Scattering from Surfactant-Assisted Aqueous Dispersions of Carbon Nanotubes. *J. Am. Chem. Soc.* **2004**, *126* (32), 9902–9903.
- (11) Shih, C.-J.; Lin, S.; Strano, M. S.; Blankschtein, D. Understanding the Stabilization of Single-Walled Carbon Nanotubes and Graphene in Ionic Surfactant Aqueous Solutions: Large-Scale Coarse-Grained Molecular Dynamics Simulation-Assisted DLVO Theory. *J. Phys. Chem. C* **2015**, *119* (2), 1047–1060.
- (12) Pang, J.; Xu, G. Molecular Dynamics Simulations of the Interactions between SWNT and Surfactants. *Comput. Mater. Sci.* **2012**, *65*, 324–330.
- (13) Tummala, N. R.; Striolo, A. SDS Surfactants on Carbon Nanotubes: Aggregate Morphology. *ACS Nano* **2009**, *3* (3), 595–602.
- (14) Tummala, N. R.; Striolo, A. Curvature Effects on the Adsorption of Aqueous Sodium-Dodecyl-Sulfate Surfactants on Carbonaceous Substrates: Structural Features and Counterion Dynamics. *Phys. Rev. E - Stat. Nonlinear Soft Matter Phys.* **2009**, *80* (2), 021408.

(15) Suttipong, M.; Tummala, N. R.; Striolo, A.; Batista, C. S.; Fagan, J. Salt-Specific Effects in Aqueous Dispersions of Carbon Nanotubes. *Soft Matter* **2013**, *9* (14), 3712–3719.

(16) Duque, J. G.; Densmore, C. G.; Doorn, S. K. Saturation of Surfactant Structure at the Single-Walled Carbon Nanotube Surface. *J. Am. Chem. Soc.* **2010**, *132* (45), 16165–16175.

(17) Wang, R. K.; Chen, W. C.; Campos, D. K.; Ziegler, K. J. Swelling the Micelle Core Surrounding Single-Walled Carbon Nanotubes with Water-Immiscible Organic Solvents. *J. Am. Chem. Soc.* **2008**, *130* (48), 16330–16337.

(18) Shastry, T. A.; Morris-Cohen, A. J.; Weiss, E. A.; Hersam, M. C. Probing Carbon Nanotube-Surfactant Interactions with Two-Dimensional DOSY NMR. *J. Am. Chem. Soc.* **2013**, *135* (18), 6750–6753.

(19) Karachevtsev, V. A.; Glamazda, A. Y.; Plokhotnichenko, A. M.; Leontiev, V. S.; Linnik, A. S. Comparative Study on Protection Properties of Anionic Surfactants (SDS, SDBS) and DNA Covering of Single-Walled Carbon Nanotubes against pH Influence: Luminescence and Absorption Spectroscopy Study. *Mater. Werkst.* **2011**, *42* (1), 41–46.

(20) Niyogi, S.; Boukhalfa, S.; Chikkannanavar, S. B.; McDonald, T. J.; Heben, M. J.; Doorn, S. K. Selective Aggregation of Single-Walled Carbon Nanotubes via Salt Addition. *J. Am. Chem. Soc.* **2007**, *129* (7), 1898–1899.

(21) Tang, X.; Koenig, P. H.; Larson, R. G. Molecular Dynamics Simulations of Sodium Dodecyl Sulfate Micelles in Water - The Effect of the Force Field. *J. Phys. Chem. B* **2014**, *118* (14), 3864–3880.

(22) Bezzobotnov, V. Yu.; Borbély, S.; Cser, L.; Faragó, B.; Gladkikh, I. A.; Ostanevich, Yu. M.; Vass, Sz. Temperature and Concentration Dependence of Properties of Sodium Dodecyl Sulfate Micelles Determined from Small-Angle Neutron Scattering Experiments. *J. Phys. Chem.* **1988**, *92* (20), 5738–5743.

(23) Phillips, J. C.; Braun, R.; Wang, W.; Gumbart, J.; Tajkhorshid, E.; Villa, E.; Chipot, C.; Skeel, R. D.; Kalé, L.; Schulten, K. Scalable Molecular Dynamics with NAMD. *J. Comput. Chem.* **2005**, *26* (16), 1781–1802.

(24) Hart, K.; Foloppe, N.; Baker, C. M.; Denning, E. J.; Nilsson, L.; MacKerell, A. D. Optimization of the CHARMM Additive Force Field for DNA: Improved Treatment of the Bi/Bii Conformational Equilibrium. *J. Chem. Theory Comput.* **2012**, *8* (1), 348–362.

(25) Denning, E. J.; Priyakumar, U. D.; Nilsson, L.; Mackerell, A. D., Jr. Impact of 2'-Hydroxyl Sampling on the Conformational Properties of RNA: Update of the CHARMM All-Atom Additive Force Field for RNA. *J. Comput. Chem.* **2011**, *32* (9), 1929–1943.

(26) Humphrey, W.; Dalke, A.; Schulten, K. VMD: Visual Molecular Dynamics. *J. Mol. Graph.* **1996**, *14* (1), 33–38.

(27) Alizadehmojarad, A. A.; Bachilo, S. M.; Weisman, R. B. Compositional Analysis of ssDNA-Coated Single-Wall Carbon Nanotubes through UV Absorption Spectroscopy. *Nano Lett.* **2022**, *22* (20), 8203–8209.

(28) Darden, T.; York, D.; Pedersen, L. Particle Mesh Ewald: An Nlog(N) Method for Ewald Sums in Large Systems. *J. Chem. Phys.* **1993**, *98* (12), 10089–10092.

TOC Graphic

